Optical coherence tomography-based scanning system for shape determination, wall thickness mapping, and inner inspection of glass containers

Eneas Nicolás Morel,[1,*] Marina Verónica Gutierrez,[1] Hernán Miguel Miranda,[1] Edgardo Luis Sambrano,[2] and Jorge Román Torga[1]

[1]Laboratorio de Optoelectrónica y Metrología Aplicada, Facultad Regional Delta, UTN, San Martín 1171, Campana 2804, Buenos Aires, Argentina

[2]Área Vidrios—Cidemat -SEGEMAR, Av. Gral. Paz 5445 E14, San Martin, Buenos Aires B1650KNA, Argentina

*Corresponding author: nmorel@frd.utn.edu.ar

Received 29 November 2012; revised 2 February 2013; accepted 4 February 2013; posted 4 February 2013 (Doc. ID 180828); published 12 March 2013

In this work we present a method that enables simultaneous measurement of shape and wall parameters of glass containers. The system is based on the optical coherence tomography technique, employing the spectral domain configuration. The data were obtained by measuring the spatial coordinates of a sequence of points in a predefined region of a sample that includes points on the surface and in the interior of the material. Dimensional parameters, thickness mapping, and tomography studies of the interior of the sample walls can be obtained from these measurements.

OCIS codes: 120.3930, 110.4500.

1. Introduction

Shape and thickness measurement, combined with flaw detection in glass containers, are important issues in the industrial inspection processes. The current quality demand in finished products requires continuous improvement in the techniques used for these processes. Determining dimensional parameters, thickness measurement, and interior analysis of container walls is of particular interest among these processes, as they provide crucial information in quality control, mechanical resistance studies, and glass-forming process research.

A great variety of methods are used to perform these measurements; among them optical methods are widely accepted, as they have the advantage of being nondestructive techniques. Currently the most frequently used systems involve artificial vision, with one or more cameras combined with different illumination configurations and a great deal of image-processing techniques and algorithms, developed for this purpose [1–4]. Based on these methods, a variety of commercial equipment is available [5]. There are more specific techniques that offer complementary information about thickness or index determination, such as laser light reflection [6] and spectral interference [7–9], in which measurements are obtained by phase change retrieval. In this paper we introduce an inspection technique based on optical coherence tomography (OCT). This technique allows us to obtain 3D images of transparent materials based on low-coherence interferometry. Nondestructive testing and materials research applications, employing OCT techniques, have been steadily growing over the past few years [10–12] in topics, such as material studies, thickness measuring, index of refraction determination, and birefringence characterization

1559-128X/13/091793-06$15.00/0

[13–15]. In this work we present this method as a proposal to obtain, simultaneously, 3D shape, wall thickness measurement, and inner studies of glass containers. The technique can be applied to studies of wall formation, nonhomogeneous glass distribution, and material resistance, as well as to the evaluation of internal flaws.

The proposed instrument is an optical head that contains a low-coherence fiber interferometer, mounted on a translation stage that is combined with a rotation stage where the sample is placed. The complete system is designed to perform combined movements to perform selective scans on the sample. With the setup used in this work, the maximum distance that can be measured with the low-coherence interferometer is 2 mm. This value, commonly known as depth range, is determined by the features of the detector of the interference signal [16]. The mechanical system was designed to scan a region up to 25 mm in height, and rotational angles between 0° and 360°, in samples with diameters up to 200 mm in length. The typical repeatability in distance measurements is 10 μm. In the following sections, general principles of the instrument and experimental results on glass containers are shown.

2. Principle of Operation and Description of the System

The idea of the technique is to achieve results by measuring the absolute spatial position of a sequence of previously selected points, on the surface or inside the sample. To perform this measuring, we proposed and built a system that consists of an optical head mounted on a vertical translation stage and a sample holder that allows a rotational movement (Fig. 1). A cylindrical coordinate system (r, θ, z) is used to assign the corresponding position to each measured point. The azimuth (θ) and the height (z) coordinates of each point are measured through a system of encoders—one in the translation stage, and the other in the rotational stage. The radial coordinate (r) is obtained indirectly from the optical path difference (OPD) value (h) obtained by low-coherence interferometry. This allows measuring the surface and inner points in the sample. For each pair of values (θ, z) the interferometric signal allows us to achieve the corresponding radial distance of the different reflections inside the sample from the outside wall to the inside wall.

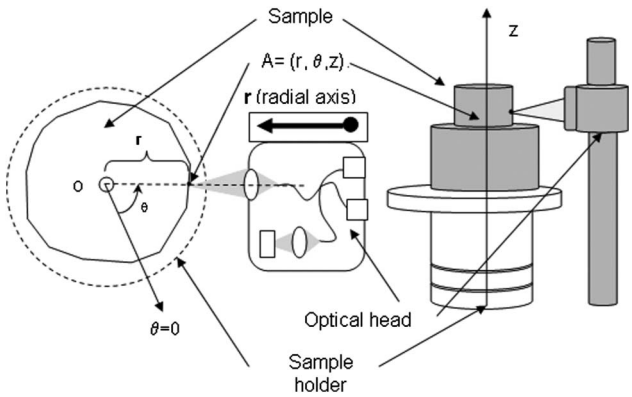

Fig. 1. Scheme showing the coordinates system, the optical head, and the sample holder with the rotation stage.

A schematic setup is shown in Fig. 1. The sequence of points measured on the sample is obtained with a coordinated movement of the roto-translational system that was designed so that the platform center and the sample's illuminated point (O and A in Fig. 1) are always in the same straight line on the radial axis.

A. Optical Head

The optical head contains a low-coherence fiber interferometer with a connection to the light source and to the detection system. We used the configuration known as Fourier-domain low-coherence interferometry (FDLCI), with a spectrometer as detector system. The head can be moved along the radial direction (r axis in Fig. 1) and along the vertical direction (z axis in Fig. 1). A detailed scheme is shown in Fig. 2. In this configuration, each measurement obtained with the interference signal (h) is the OPD between the point illuminated in the sample (A in Fig. 1) and the reference surface position (RS, in Fig. 2) that is located in the optical head.

In a simplified situation in which there is only one reflection in the sample, the interference signal can be written as [17]

$$I(k) = I_0(k)(1 + \beta^2 + \beta \cos(k \cdot h)), \tag{1}$$

where $I_o(k)$ and $\beta^2 I_o(k)$ are the power spectral density reflected from the reference and sample arms, respectively, k is the wave number, and h is the corresponding OPD between the reference mirror and the sample. In the conjugate space,

$$\mathrm{FT}(I)(H) = \Gamma(H) \otimes (\delta(H) + \beta' \cdot \delta(H - h) + \beta' \cdot \delta(H + h)), \tag{2}$$

where H is the conjugate coordinate of k, $\Gamma(H)$ is the coherence function linked with power spectral density according to the Wiener–Kinchin theorem, and β and β' are constant factors related to reflectivity of the surfaces.

B. Calibration Interference Signal and Obtaining the Radial Coordinate

To obtain the radial coordinate of each measured point in the sample, a two-step procedure is required. The first step is calibration of the low-coherence interferometer [18]. The second step is to obtain a conversion relationship to get the r coordinate from the h value previously obtained. Calibration of the spectrometer is performed by controlled movement of a reference mirror, which is done with a translational stage (y axis in Fig. 2) placed inside the optical head. The same system allows us to set the $h = 0$

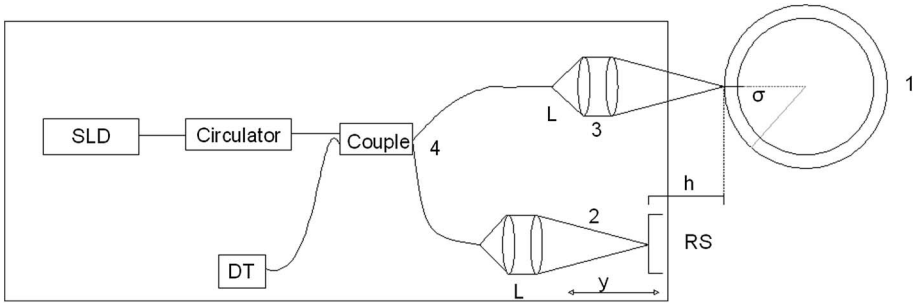

Fig. 2. General scheme of the optical head: 1, sample; 2, reference arm; 3, sample arm; 4, fiber beam splitter; SLD, superluminiscent diode; DT, spectrometer; RS, Reference arm surface; L, focus lens.

value in order to employ the complete dynamic range of the interferometer.

It is possible to extend the measurement range in the radial axis with an additional mechanical movement of the optical head along the radial direction (r axis displacement in Fig. 1). We did not use this movement in the experimental results shown above (Section 3).

A referential surface, placed as a sample, is used to convert the h value into the radial coordinate r. In this work a metallic cylindrical surface with known radius was employed. The surface was scanned in a full rotation, maintaining its height (z). A sequence of the same pitch angled points was measured with the optical head. This provides an overdetermined set of measurements, which is fitted applying a nonlinear least-squares algorithm, to obtain the conversion from the h to the r value. Figure 3 shows the measured points and the fitting curve obtained on a cylindrical surface with a radius of 15 ± 0.10 mm. The r value obtained from the fitting process is 14.99 ± 0.20 mm. The error in the r axis was estimated as the average dispersion between the measured values and the values obtained using the fitted curve. The calculus was made with the same sequence of points used to obtain the h to r conversion value (Fig. 3).

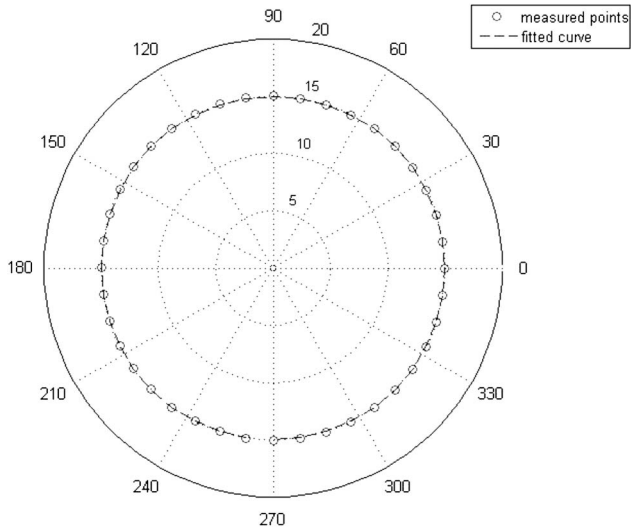

Fig. 3. Sequence of measured points in a complete turn of a cylindrical surface (reference) and the fit curve used to obtain the OPD (h) to radial coordinate (r) conversion.

An additional mechanical movement of the optical head in the radial axis, if it is necessary in the measurement process, is registered by an encoder located in the translation stage (radial axis displacement in Fig. 1). So the actual radial coordinate of the point measured in the sample is corrected considering this displacement.

C. Experimental Setup

The interferometer is a fiber Michelson type, with a circulator and a coupler fiber system (AC Photonics). The light source is a superluminescent diode (Superlum, model SLD 351 HP3), centered around 840 nm, with a 60 nm spectral width. A fiber collimator (Thorlabs CFC-2x-B) and a different focus lens were used at the end of the sample arm (3 in Fig. 2). A collimator (Thorlabs CFC-2x-B) and a mirror, which can be linearly displaced (y axis), were used as the reference arm (2 in Fig. 2). The interval range on the y axis is 25 mm in our system. The detection system is a HR4000 Ocean Optics spectrometer, with an operating interval from 700 to 900 nm.

The linear displacement system (z axis) is a linear stage (SMA-25pp Newport), which allows 25 mm displacements with a precision of 5 μm. The rotational system was specifically designed to be used in this setup and allows us to perform any rotation with steps varying from 0.5° to 5° and a $9 \cdot 10^{-3}$° resolution (Encoder Products, model 15T01SB-000013). The system admits samples with a radius up to 200 mm.

The optical head can be moved in the radial axis (r axis in Fig. 1) in order to position over the sample's surface (SMA-25pp Newport linear stage).

3. Measurements and Results

The measurements were made on vials employed in the pharmaceutical industry with the objective to obtain dimensional parameters, width wall mapping, and characterization of the internal bubbles, as an example of the potential of this technique for determining internal flaws.

The system of Fig. 1 was used to obtain all the measurements by performing a convenient scanning on a selected region of the sample.

A typical measurement is shown in Fig. 4. The curve is the fast Fourier transform of the

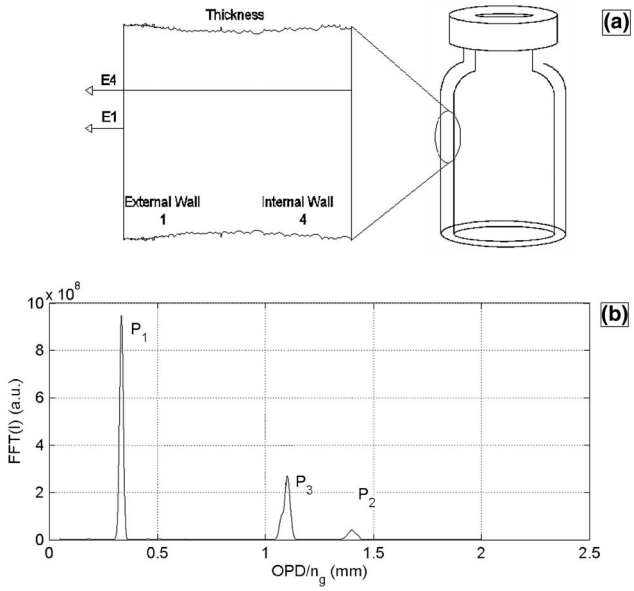

Fig. 4. (a) Schematic of the sample and the optical fields at the sample arm. (b) FFT(I) as a function of the normalized optical path distance, for a typical measurement. (An arbitrary zero was selected for the horizontal axis).

interference signal [FFT(I)] obtained from a reflection in a particular point in the sample.

The reflections on the exterior wall (E_1) and the inner wall (E_4) of the sample, and a third reflection in the reference mirror (E_r) placed in the optical head, generate an interference signal whose FFT is shown in Fig. 4. The horizontal axis is the normalized OPD (OPD/ng), where ng represents the group refractive index of the corresponding material. The center coordinates of each of the three peaks (P_1, P_2, P_3) shown in Fig. 4 are the corresponding OPD values—$h1, h2$, and $h3$—which in this experiment are

$$h_1 = \mathrm{OPD}(E_1E_r),$$
$$h_2 = ng \cdot d = \mathrm{OPD}(E_1E_4),$$
$$h_3 = h1 + ng \cdot d = \mathrm{OPD}(E_4E_r).$$

In samples having multiple interfaces (as in Fig. 4), the expression for $I(k)$ includes terms that correspond to the interference of the reflected reference beam and beams reflected from interfaces distributed within the sample, commonly known as cross-correlation terms. In the same expression, there are also terms associated with the interference between beams reflected from different sample interfaces, also known as autocorrelation terms. In the analysis for recovering sample structure, it is necessary to identify, in the Fourier transform of $I(k)$, peaks due to the cross-correlation terms (P1 and P3 in Fig. 4) and peaks due to the autocorrelation terms (P2 in Fig. 4). This can be done by comparing the FFT(I) curve when two interferometer arms are present and when the reference arm is blocked or by increasing the distance from the reference surface to the sample, with the drawback of decreasing the depth range. Alternatively, phase shifting can be used to eliminate the autocorrelation terms, as was implemented in differential Fourier-domain OCT [19].

Figure 5 shows the thickness wall mapping, for a fixed value of z, in a complete turn of the sample.

Figure 6 shows the result of a complete scan performed in a sector of a similar sample. This scanning was performed in a section 10 mm in height. The measurement was accomplished by selecting points in steps of 1 mm in the z direction and with 9° angular pitch. A complete turn ($0 < \theta < 360°$) for each z value was scanned. Specific software was developed to integrate each measurement with the radial conversion described above and with the azimuth and height values measured by the encoders located in the translational and rational stages. With these values, dimensional parameters of the scanned region can be obtained.

The time used to perform a typical measurement, as in the examples shown in Figs. 5 and 6, can be estimated, taking into account that the measuring time of each point with the interferometer is approximately 4 ms, to which must be added the time necessary to move the optical head of a point to the next point. A measurement of wall thickness in one complete turn of the sample (400 points) takes 4 min. The time for a scan of a portion of the sample, as in Fig. 6 with 4000 points, is 45 min.

A. Characterization of an Internal Bubble

In this section we show a characterization of an internal bubble, as an application of this technique

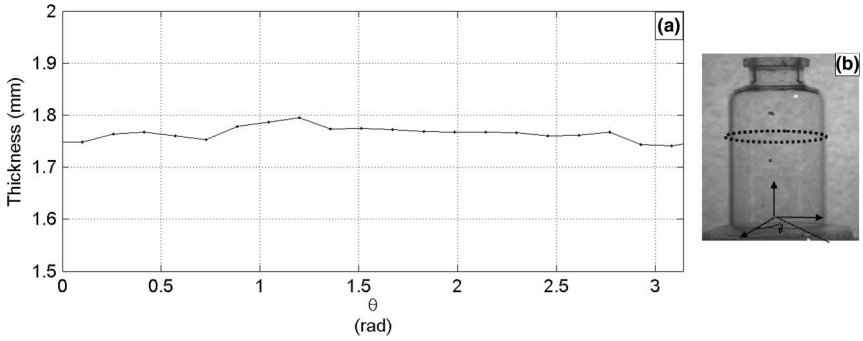

Fig. 5. (a) Thickness of the container wall as a function of the angle θ (defined as in Fig. 1) for a constant z value. (b) Photo of the sample.

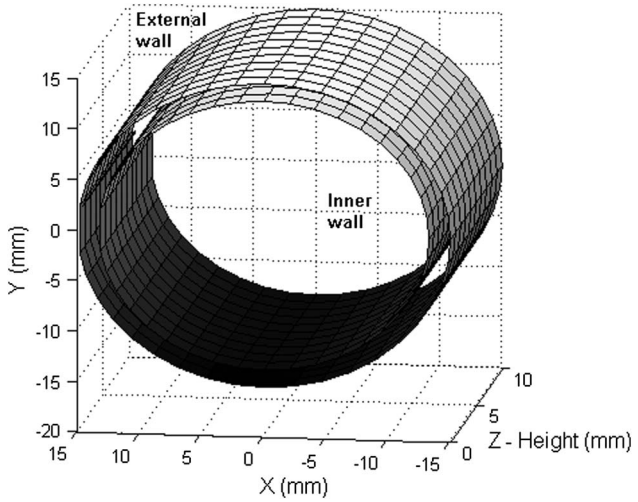

Fig. 6. 3D image of a sector of the sample shown in Fig. 5(b). The Y, X, and Z axes are placed only for clarity.

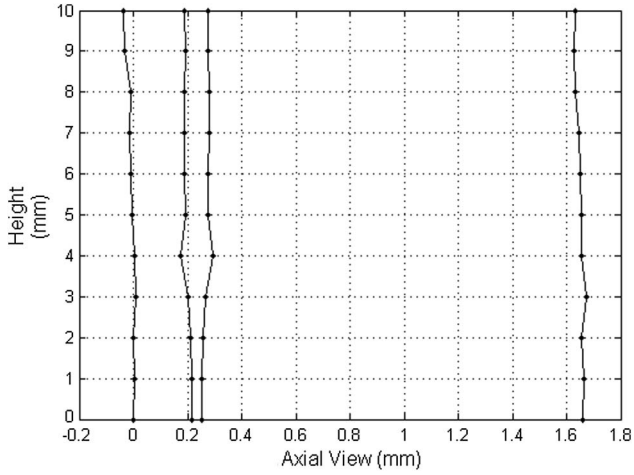

Fig. 8. Reconstruction of the bubble shape and its location within the sample. An arbitrary zero in the external wall position was selected for the radial distance.

to obtain data from the interior of the container walls. The measurement was performed with the same scheme shown in Fig. 1.

Figure 7(a) shows reflections at the various interfaces of the sample. Figure 7(b) shows the FFT of the interference signal produced with these reflections. For clarity the reference arm was blocked and the center coordinates of each of the three peaks (P_1, P_2, and P_3) shown in the figure are the corresponding OPD values:

$$h_1 = \mathrm{OPD}(E_1E_2),$$
$$h_2 = \mathrm{OPD}(E_1E_3),$$
$$h_3 = ng \cdot d = \mathrm{OPD}(E_1E_4).$$

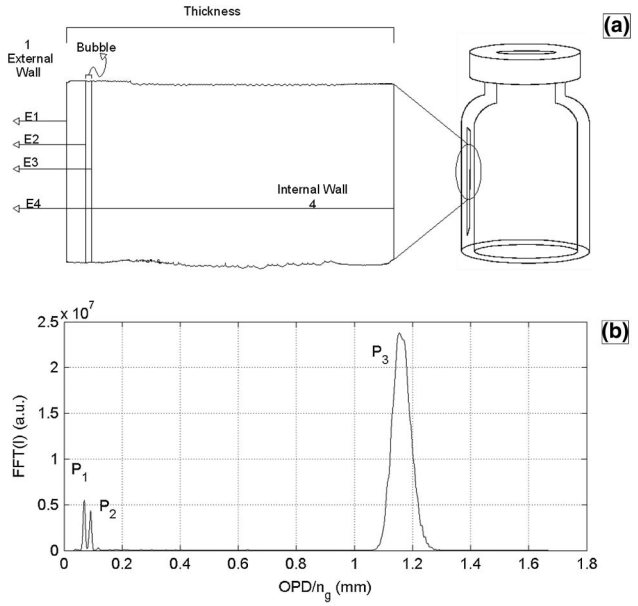

Fig. 7. (a) Schematic of the sample and the optical fields at the sample arm. (b) FFT(I) as a function of the OPD (h) for a typical measurement.

By carrying out a vertical scan (in z), the bubble's size and its position inside the sample can be obtained as shown in Fig. 8.

4. Conclusions

We introduce and demonstrate a system that enables simultaneous measurement of the dimensional shape and wall parameters of glass containers. The technique offers interesting alternatives that, to the best of our knowledge, are not found in previous works or in currently used equipment [5]. By utilizing FDLCI and the proposed mechanical design, it is possible to obtain the spatial coordinates of different points measured in the sample. It was shown that from these measurements it is possible to obtain a 3D image of the sample that provides the parameters of interest proposed in this paper, using thickness mapping and the dimensional distances. Such images have high resolution and large depth range compared with those obtained with other optical techniques.

With the experimental setup employed in this work, it was possible to scan regions that were 25 mm in height, had an azimuth angle between 0° and 360°, and were up to 2 mm in thickness (radial axis) in samples with a diameter up to 80 mm in length. The error in the distance measurement obtained with the interference signal (h) is 2 μm, and the error in the radial coordinate is 200 μm. To reduce this error, it is necessary to improve the accuracy of the cylindrical gauge used as the referential surface. No evaluation was made using this equipment in conditions of noise as in an industrial environment. However, proper use of the equipment in conditions similar to those in a metrology room has been demonstrated.

The potential of this technique as a nondestructive test for container glasses was also shown by measuring the position and dimension of an internal bubble.

The use of multiple optical heads in one measuring station reduces inspection time and also offers the

interesting alternative of employing heads with different characteristics (focus distance and positioning system) aimed at specific applications. Future work will seek to improve the technique to go in this direction for application in the packaging industry.

The authors gratefully acknowledge the financial support provided to this study by the Universidad Tecnológica Nacional, Argentina, under grant PID UTI1113, and the Agencia Nacional de Promoción Científica y Tecnológica, Argentina, under grant PICT 2128-2006. E. N. Morel and J. R. Torga are members of CONICET, Argentina.

References

1. M. Canivet, R. D. Zhang, and M. Jourlin, "Finish inspection by vision for glass production," Proc. SPIE **2183**, 164–169 (1994).
2. H. Liu and Y. Wang, "Development of glass bottle inspector based on machine vision," presented at the 10th International Conference on Control, Automation, Robotics and Vision, Hanoi, Vietnam, 17–20 December 2008.
3. M. Carrasco, L. Pizarro, and D. Mery, "Image acquisition and automated inspection of wine bottlenecks by tracking in multiple views," in *Proceedings of the 8th International Conference on Signal Processing, Computational Geometry and Artificial Vision (ISCGAV) 2008*(World Scientific, 2008), pp. 82–89.
4. Z. Wen, J. Ge, L. Xia, Y. Luo, and Z. Chen, "Fast online detection of body defect of glass containers," Proc. SPIE **8201**, 82011 (2011).
5. http://www.krones.com/en/index.html; http://www.emhartglass.com/cold-end.
6. J. Laurent and L. Francis, "Method for measuring three-dimensional objects by single-view optical shadowgraphy, using the optical laws of light propagation," U.S. patent 7,880,898 (1 February 2011).
7. V. N. Kumar and D. N. Rao, "Using interference in the frequency domain for precise determination of thickness and refractive indices of normal dispersive materials," J. Opt. Soc. Am. B **12**, 1559–1563 (1995).
8. R. Nitsche and T. Fritz, "Correct interpretation of spectral interference measurements of weakly absorbing films of micrometer thickness," Opt. Lett. **29**, 938–940 (2004).
9. P. Hlubina, D. Ciprian, J. Lunácek, and M. Lesnák, "Dispersive white-light spectral interferometry with absolute phase retrieval to measure thin film," Opt. Express **14**, 7678–7685 (2006).
10. http://www.octnews.org/category/14/non-medical/.
11. D. Stifter, "Beyond biomedicine: a review of alternative applications and developments for optical coherence tomography," Appl. Phys. B **88**, 337–357 (2007).
12. D. Stifter, K. Wiesauer, M. Wurm, E. Leiss, M. Pircher, E. Götzinger, B. Baumann, and C. Hitzenberger, "Advanced optical coherence tomography techniques: novel and fast imaging tools for non-destructive testing," presented at *The 17th World Conference on Nondestructive Testing*, Shanghai, China, 25–28 October 2008. http://www.ndt.net/article/wcndt2008/papers/456.pdf.
13. V. Srivastava, T. Anna, M. Sudan, and D. Singh Mehta, "Tomographic and volumetric reconstruction of composite materials using full-field swept-source optical coherence tomography," Meas. Sci. Technol. **23**, 055203 (2012).
14. D. F. Murphy and D. A. Flavin, "Dispersion-insensitive measurement of thickness and group refractive index by low-coherence interferometry," Appl. Opt. **39**, 4607–4615 (2000).
15. S. H. Kim, S. H. Lee, J. I. Lim, and K. H. Kim, "Absolute refractive index measurement method over a broad wavelength region based on white-light interferometry," Appl. Opt. **49**, 910–914 (2010).
16. N. Nassif, B. Cense, B. Park, M. Pierce, S. Yun, B. Bouma, G. Tearney, T. Chen, and J. de Boer, "In vivo high-resolution video-rate spectral-domain optical coherence tomography of the human retina and optic nerve," Opt. Express **12**, 367–376 (2004).
17. T. Bajraszewski, M. Wojtkowski, M. Szkulmowski, A. Szkulmowska, R. Huber, and A. Kowalczyk, "Improved spectral optical coherence tomography using optical frequency comb," Opt. Express **16**, 4163–4176 (2008).
18. Z. Hu, Y. Pan, and A. M. Rollins, "Analytical model of spectrometer-based two-beam spectral interferometry," Appl. Opt. **46**, 8499–8505 (2007).
19. M. Wojtkowski, R. Leitgeb, A. Kowalczyk, T. Bajraszewski, and A. F. Fercher, "In vivo human retinal imaging by Fourier domain optical coherence tomography," J. Biomed. Opt. **7**, 457–463 (2002).